Development of Multi Field Software Solutions and their Application for the Optimization of Electromagnetic High Speed Forming processes[*]

M. Stiemer[1], B. Svendsen[2], J. Unger[2], F. T. Suttmeier[1], H. Blum[1]

[1]Chair of Scientific Computing, University of Dortmund
[2]Chair of Mechanics, University of Dortmund

Abstract

The simulation of complex processes in engineering solids involving coupled mechanical and non-mechanical fields represents a challenge to physicists, mathematicians, and engineers. Both, the formulation of such models and their numerical implementation involve a great number of difficulties. Electromagnetic forming is one example of such a process, whose modelling and simulation requires a coupled electromagnetic-thermomechanical model. The purpose of this contribution is to discuss some key issues associated with the modelling and simulation of electromagnetic metal forming (EF) and the corresponding development of a finite-element-based simulation tool for EF. In particular, the modelling is based on a thermodynamically-consistent electromagnetic-thermoelastoviscoplastic material and field model in which the energy and momentum balance are coupled to the quasi-static form of Maxwell's equations via the electromotive intensity and Lorentz force, respectively. On the algorithmic side, questions like the choice of meshes, the element formulation, the numerical treatment of nonlinearities, possible model simplifications, different discretisation strategies, realisation of the non-linear coupling etc. are discussed for the presented software solution. Such issues are investigated with the help of benchmark simulations that have been developed for this purpose. Finally, as an example of an application of the developed software tool, a computer–aided–manufacturing (CAM) problem is considered. Here, the size of the tool coil and the peak value of the current in the tool coil circuit are optimised in order to achieve the prescribed work-piece form within the given tolerance.

Keywords:

Modelling, Viscoplasticity, Electromagnetic metal forming

---

1   Introduction

Electromagnetic metal forming (EF) is a high-speed forming process achieving strain rates of $\varphi_v \geq 10^3$ 1/s. In this method, a strong pulsed magnetic field is generated in the tool coil adjacent to an electrically-conducting work-piece to be formed. The interaction of the induced eddy currents in the work-piece with the magnetic field generates a Lorentz (body) force in the work-piece resulting in its deformation. The entire resulting highly dynamical forming process lasts on the order of 100-300 μs. EF represents an effective forming method for metals with good electrical conductivity like aluminum or copper. Compared to other forming methods, it offers advantages such as an increase in formability for certain kinds of materials, reduction in wrinkling, the ability to combine forming and assembly operations, reduced tool-making costs, *etc.*. Nevertheless, EF, is not yet sufficiently well understood to be routinely used as industrial forming process. In particular, further investigation of the strong dependence of the forming process on the details of the interaction between the transient magnetic field and evolving shape of the work-piece is needed, representing one purpose of the current work.

Beyond physically-reasonable models, such investigations require the availability and use of a reliable simulation tool for coupled multifield problems. The introduction of high-speed computers in the late 80's enabled the first numerical simulation of EF including the deformation of the work-piece. In contrast to Goudin [1, 2], the interaction between the magnetic field and the shape of the work-piece is considered in Takata [3]. In his approach, the influence of the change of shape of the work-piece during the electromagnetic forming process on the magnetic field, and the force it exerts on the work-piece are therefore modelled correctly. Fenton and Daehn [4] used the computer-code CALE [5] to simulate electromagnetic forming with complete magnetomechanical coupling numerically. Further, Beerwald *et al.* [6, 7] have used the commercial program MARC [8] to simulate electromagnetic forming processes. Recently, electromagnetic sheet metal forming has been investigated by Badelt *et al.* [9] and Beerwald *et al.* [10], respectively. In Beerwald *et al.* [10], both, a time harmonic simulation of the electromagnetic field using the finite-element programme FEMM [11] and a transient simulation using the finite-element programme EMAS [12] were combined with the simulation of the sheet metal deformation using the finte-element programme MARC [8]. Although viable, the black-box nature of these programmes as well as the required interfacing of these "by hand" to carry out the complete simulation is not terribly efficient nor sufficiently flexible to be able to incorporate new models and numerical methods needed to improve the realism, efficiency, and robustness of the numerical simulation. To this end, as well as in order to combine all aspects of the modelling and simulation of EF into one integrated, unified software environment, the finite element code SOFAR (**S**mall **O**bject orientated **F**inite-element-library for **A**pplication and **R**esearch) (SOFAR: [13]) has been applied and developed by a research group (FOR 443) in Dortmund, funded by the German Research Foundation (DFG). The underlying thermodynamically-consistent electromagnetic thermoinelastic multifield model has been developed in [14, 15]. The corresponding algorithmic formulation and efficient numerical implementation has been carried out and discussed in [16]. In work in progress, a number of benchmark simulations, such as those reported on in [17], are being systematically carried out in order to test the efficiency and numerical robustness of the new SOFAR-based simulation tools.

The purpose of the current work is to outline and discuss various issues involved in the

development and use of SOFAR as a tool for the simulation of EF. From the modelling point of view, SOFAR is used in particular for model identification and validation in the context of comparison with experimental results [9, 10]. On the algorithmic side, several different approaches have been tested and validated (see section 3). Moreover, the applicability of SOFAR to the simulation of optimisation and design problems is currently being investigated. As an example of this, the peak value of the current in the tool coil circuit is optimised in such a way that electromagnetically-formed sheet metal achieves a prescribed form within a given tolerance. The corresponding optimisation is based on a numerical method from [18] which converges for a wide class of objective functions. Moreover, no derivatives have to be computed. Such possibilities represent first steps in the development of computer-aided-manufacturing (CAM) methods based on SOFAR.

2 Coupled Model for Conducting, Thermoelastoviscoplastic Metals

The multifield material model used in the current work is derived from a general continuum thermodynamic approach [15] to the formulation of models for electromagnetic thermoinelastic solids. In particular, this model applies to the case in which a strong magnetic field induces electric currents in thermoelastoviscoplastic electric conductors and so a Lorentz force resulting in their deformation. This is the basic idea underlying the method of electromagnetic metal forming. Now, for all structural problems of interest, the frequencies of relevance (*i.e.*, less than 10 MHz) correspond to electromagnetic wavelengths which are much larger than the structures of interest. As such, the wave character of the electromagnetic fields is insignificant and can be neglected for such structural problems. This represents the so-called quasistatic approximation [19, §2.2 and §8.2]. In this case, it is shown in [15] that Maxwell's relations together with Ohm's law and the Coulomb gauge condition (*e.g.*, [20], §6.5) result in the weak forms[*]

$$\int_R \overset{*}{a} \cdot a_* + (\chi - a \cdot v)\, \operatorname{div} a_* + \kappa_{\mathsf{EM}} \operatorname{curl} a \cdot \operatorname{curl} a_* \;=\; 0\,,$$

$$\int_R \chi\, \operatorname{div}(\nabla \chi_*) \;=\; 0\,,$$

(1)

for the usual vector a and the scalar χ potentials with respect to a spatial region R containing the work-piece and tool coil for the special case that a and χ are specified everywhere on ∂R. Here, a_* and χ_* represent test fields vanishing on those parts of the boundary ∂R of R where a and χ are specified.

Moreover, $\kappa_{\mathsf{EM}} := \sigma_{\mathsf{EM}}^{-1} \mu_{\mathsf{EM}}^{-1}$ represents the magnetic diffusivity, σ_{EM} the electrical conductivity, and μ_{EM} the magnetic permeability. In addition, v represents the spatial velocity of the work-piece or tool coil, $\dot{f} := \partial f + \nabla f \cdot v$ the material time derivative, $D := \operatorname{sym}(L)$ the deformation rate, and $L := \nabla v$ the velocity gradient. Further, $\overset{*}{a} := \dot{a} + L^{\mathsf{T}} a = \partial a + (\nabla a)v + L^{\mathsf{T}} a$ represents the objective time-derivative of a. On the timescale $\tau_{\mathsf{Exp}} \sim 10^{-4}$ s relevant to processes such as electromagnetic metal forming, the typical order of magnitude $\kappa_{\mathsf{EM}} \sim 10^{-1}$ m^2 s^{-1} for the magnetic diffusivity of metals implies that "significant" magnetic diffusion takes

---

[*]The volume dv and surface da elements are dispensed with in the corresponding integrands in this work for notational simplicity.

place over lengthscales of $\sqrt{\kappa_{\mathsf{EM}} \tau_{\mathsf{Exp}}} \sim 10$ cm. Since this is significantly larger than the smallest dimension of the engineering structures of interest (*e.g.*, sheet metal thickness ~ 1 mm), magnetic diffusion will be important in the applications to be discussed below.

Restricting attention to the case of axisymmetry, note that the above field equation for the vector potential a reduces to a scalar equation for the azimutal component a_φ of a and a Laplace equation $\Delta\chi = 0$ for the scalar potential χ. Indeed, since the flux density is constant in azimuthal direction, the vector potential is always perpendicular to the rz–plane, where r denotes the radial component and z the axial. In particular, this implies that the Coulomb gauge condition div $a = 0$ is always fulfilled, and thus the equations for a and χ decouple. In this case, standard nodal finite elements can be utilised. For three-dimensional problems, however, special elements are required which can deal with jump discontinuities in the vector potential field a (*e.g.*, [27, 28, 29]).

As discussed in [15], to a good first approximation, adiabatic conditions pertain during electromagnetic forming. In this case, the energy balance reduces to the evolution relation

$$\dot{\theta} = \varrho^{-1} c^{-1} (\omega + \sigma_{\mathsf{EM}} \epsilon \cdot \epsilon) \tag{2}$$

for the temperature, where ϱ represents the mass density, c the specific heat, ω the mechanical rate of heating, and ϵ the electromotive intensity. In the adiabatic approximation, then, the temperature becomes homogeneous and can be treated formally as an internal variable (see below). As such, the deformation ξ is the only thermomechanical field. The weak balance relation for momentum is given by

$$\int_{B_{\mathsf{r}}} \{\varrho_r \ddot{\xi} - \det(F) \sigma_{\mathsf{EM}} \epsilon \times \operatorname{curl} a\} \cdot \xi_* + K \cdot \nabla\xi_* = \int_{\partial B_{\mathsf{c}}} t_c \cdot \xi_* \tag{3}$$

with respect to the reference $B_{\mathsf{r}} \subset R$ configuration of the work-piece or tool coil for all corresponding test fields ξ_* vanishing on those parts of the boundary ∂B_{c} of the current configuration $\partial B_{\mathsf{c}} \subset R$ where ξ is specified. Here, ϱ_r represents the referential mass density, $F := \nabla\xi$ the deformation gradient, K the Kirchhoff stress, and t_c the current traction vector. Note that the second term in (3) represents the Lorentz force.

Lastly, the model relations are completed by the material model. Perhaps the simplest model relevant to the case of electromagnetic forming in this regard is thermoelastoviscoplasticity with isotropic hardening. The relevant internal variables are then the elastic left Cauchy-Green deformation B_{E} and the accumulated inelastic strain ϵ_{P}. On this basis, the thermodynamic formulation being pursued here ([15]) is based on specific model relations for the referential free energy density ψ as well as on the evolution relations for the internal variables. In particular, assuming for simplicity that the elastic behaviour is not affected by inelastic processes such as damage (*e.g.*, [24]), the split[*]

$$\psi(\theta, B_{\mathsf{E}}, \epsilon_{\mathsf{P}}) = \psi_{\mathsf{E}}(\theta, B_{\mathsf{E}}) + \psi_{\mathsf{P}}(\theta, \epsilon_{\mathsf{P}}) \tag{4}$$

of the free energy into thermoelastic and inelastic parts is justified. Assuming further for simplicity that the specific heat capacity c is constant, (*e.g.*, [22]), the form

$$\psi_{\mathsf{P}}(\theta, \epsilon_{\mathsf{P}}) = \varepsilon_{\mathsf{P}}(\epsilon_{\mathsf{P}}) - \theta \, \eta_{\mathsf{P}}(\epsilon_{\mathsf{P}}) \tag{5}$$

---

[*]In the current activation/transition-state context, the temperature dependence of the dynamic flow stress is contained in the inelastic potential; see (9) below.

for the inelastic part ψ_P of ψ is obtained. Here, ε_P represents the stored energy and η_P the entropy of cold work (see also [21]). In addition, the thermoelastic neo-Hooke form

$$
\begin{aligned}
\psi_\mathrm{E}(\theta, \boldsymbol{B}_\mathrm{E}) \;=\; & \tfrac{1}{8}\,\lambda_r\,(\ln J_{\boldsymbol{B}_\mathrm{E}})^2 - \tfrac{1}{2}\,(3\lambda_r + 2\mu_r)\,\alpha_r\,(\theta - \theta_r)\,\ln J_{\boldsymbol{B}_\mathrm{E}} + \tfrac{1}{2}\,\mu_r(I_{\boldsymbol{B}_\mathrm{E}} - 3 - \ln J_{\boldsymbol{B}_\mathrm{E}}) \\
+ \;\; & \varrho_r c_r\,[\theta - \theta_r - \theta\,\ln(\theta/\theta_r)]
\end{aligned}
\tag{6}
$$

for the referential free energy density pertains, where λ_r and μ_r represent Lamé's constants, and θ_r a reference temperature. As for the inelastic part ψ_P, this is determined empirically with the help of experimental data, as discussed in the next section (see also [22]). Consider next the evolution of the internal variables and the inelastic behaviour. In the metallic polycrystalline materials of interest at low-to-moderate homologous temperature, inelastic deformation processes are controlled predominantly by the activation of dislocation glide on glide systems (*e.g.*, [23]), even at higher strain-rates. As such, higher homologous temperatures are required for other mechanisms such as dislocation climb or even dynamic recrystallisation to activate. Resistance to dislocation glide arises due to extended obstacles generating longer-range stress fields related in the phenomenological context to hardening behaviour. In addition, such resistance is caused by short-range local obstacles which can be overcome by thermal fluctuation under the action of the local effective stress, represented in the current phenomenological context by $|\mathrm{dev}(\boldsymbol{K})| + \varsigma_\mathrm{P}$, where

$$
-\varsigma_\mathrm{P} := \psi_{,\,\epsilon_\mathrm{P}} = -\theta\varrho_r\eta_{\mathrm{P},\,\epsilon_\mathrm{P}}
\tag{7}
$$

represents the static contribution to the flow stress (in shear). On this basis,

$$
f_\mathrm{P}(\theta, \epsilon_\mathrm{P}, \boldsymbol{D}, \boldsymbol{K}, \varsigma_\mathrm{P}) := \frac{|\mathrm{dev}(\boldsymbol{K})| + \varsigma_\mathrm{P}}{\sigma_\mathrm{P}(\theta, \epsilon_\mathrm{P}, \boldsymbol{D})}
\tag{8}
$$

represents an activation function or non-dimensional overstress in the current rate-dependent context. Here, σ_P represents the dynamic drag contribution to the effective flow stress in the system. On this basis, a power-law approximation of the more exact transition-state-based micromechanical relations for the kinetics of dislocation glide (*e.g.*, [23]) leads to the power-law form

$$
\phi(\theta, \epsilon_\mathrm{P}, \boldsymbol{D}, \boldsymbol{K}, \varsigma_\mathrm{P}) = \frac{\gamma_\mathrm{P}(\theta, \epsilon_\mathrm{P}, \boldsymbol{D})\,\sigma_\mathrm{P}(\theta, \epsilon_\mathrm{P}, \boldsymbol{D})}{m_\mathrm{P}(\theta, \epsilon_\mathrm{P}, \boldsymbol{D}) + 1}\,\langle f_\mathrm{P}(\theta, \epsilon_\mathrm{P}, \boldsymbol{D}, \boldsymbol{K}, \varsigma_\mathrm{P})\rangle^{m_\mathrm{P}(\theta, \epsilon_\mathrm{P}, \boldsymbol{D}) + 1}
\tag{9}
$$

upon which the evolution of the internal variables is based. Here, γ_P represents a characteristic strain-rate, $\langle x \rangle := \tfrac{1}{2}\,(x + |x|)$ the MaCauley bracket, and m_P the strain-rate exponent. Since $|x|$ is a convex function of x, note that $\langle x \rangle$ is as well. In contrast to the general form, (9) has been assumed explicitly independent of $\boldsymbol{B}_\mathrm{E}$ in this simple case. More generally, *e.g.* for the case of deformation-induced anisotropic flow behaviour, this is no longer so (*e.g.* [24, 25, 26]). From (9), we have the specific forms

$$
\begin{aligned}
\overset{*}{\boldsymbol{B}}_\mathrm{E} \;&=\; -2\,\mathrm{sym}(\phi_{,\,\boldsymbol{K}}\,\boldsymbol{B}_\mathrm{E}) \;&=\; -2\,\mathrm{sgn}(\mathrm{dev}(\boldsymbol{K}))\,\boldsymbol{B}_\mathrm{E}\,\varpi_\mathrm{P} \quad (\boldsymbol{K} \neq \boldsymbol{0})\,, \\
\dot{\epsilon}_\mathrm{P} \;&=\; \phi_{,\,\varsigma_\mathrm{P}} \;&=\; \gamma_\mathrm{P}\,\langle f_\mathrm{P}\rangle^{m_\mathrm{P}} \quad (f_\mathrm{P} > 0)\,,
\end{aligned}
\tag{10}
$$

for the evolution of the internal variables. In the current adiabatic context, the temperature θ is also treated formally as such a variable with evolution relation (2). Now, for the case of incompressible material behaviour, we assume that the isotropic forms of the viscoplastic

parameters γ_P, σ_P and m_P are independent of the trace $\boldsymbol{I} \cdot \boldsymbol{D}$ of the rate of deformation. In this case, the thermoelastic form

$$\boldsymbol{K} = 2\,\psi_{,\,B_E}\,B_E \tag{11}$$

for the Kirchhoff stress holds. In addition,

$$\omega_r = \gamma_P\,(\sigma_P f_P - \theta\,\varrho_r \eta_{P,\,\epsilon_P})\langle f_P\rangle^{m_P} - (3\lambda_r + 2\mu_r)\,\alpha_r\,\theta\,\overline{\ln \det(\boldsymbol{F})} \tag{12}$$

then follows for the referential form of the mechanical heating rate. As indicated, ϕ is differentiable in ς_P everywhere except at $f_P = 0$, and in $\boldsymbol{K}$ everywhere except at $f_P = 0$ and at $\boldsymbol{K} = \boldsymbol{0}$. The corresponding subdifferentials exist everywhere. In the context of these forms for the evolution of the internal variables, the constraint $\gamma_P(\theta, \epsilon_P, \boldsymbol{0}) = 0$ on the constitutive form of γ_P follows in thermodynamic equilibrium.

This completes the basic model formulation. Its reduction to the case of small elastic strain, algorithmic formulation and numerical implementation in SOFAR have been carried out in [16]. Aspects of this are discussed in the next section.

3   Algorithmic Implementation of the Coupled Simulations in SOFAR

The idea behind the software environment SOFAR is to reduce the development time for finite-element-based algorithms and simulation by object orientation. Hence, the interface to the developer is implemented in JAVA. On the other hand, time critical jobs like basic linear algebra (BLAS-) operations are implemented in fast native C and FORTRAN code, respectively, that can be called from JAVA routines. The programing concept of SOFAR allows easy handeling of unstructured meshes. Such meshes are typical for adaptive refinement and remeshing strategies. In particular, SOFAR administrates geometric singularities as hanging nodes. The assembly of the corresponding stiffness matrices is done automatically. Moreover, SOFAR allows access to any geometric substructure of a particular element. This means edges or faces can be addressed at any time. The latter makes it easy to implement edge elements for instance which avoid the typical problems nodal elements exhibit in 3D electromagnetic field computation [27, 28]. Moreover, effective algorithms like multigrid solver or error estimators are available. SOFAR can easily be extended by external routines (written in C or FORTRAN) due to a user interface. This user interface was applied for the implementation of the above described coupled model. Its availability in SOFAR enables the implementation and use of various custom-tailored element formulations based on modern numerical methods.

Due to the vastly different timescales associated with changes in the electromagnetic and thermomechanical fields, the corresponding field relations are solved on separate finite-element meshes via a staggered solution algorithm. In particular, the electromagnetic field relations are solved on a fixed Eulerian mesh discretising the region of space containing the work-piece and tool coil. On the other hand, the momentum and energy balances for the work-piece are solved on a Lagrangian mesh using an implicit element formulation for the thermomechanical model discussed in the last section which is embedded into SOFAR via a user-element interface. Information concerning the evolving Lorentz force, electromotive power, and changing work-piece geometry are mapped back and forth between the two meshes during the solution procedure with the help of transfer operators. SOFAR provides an object oriented concept for

the necessary bookkeeping of element data and provides the input data to the user element. Moreover, the assembly of the stiffness matrix for the Newton iteration on structural level is performed by SOFAR. Use of this staggered scheme increases the stability of the simulation and reduces numerical efforts, as global remeshing is not necessary. However, adaptive local refinement in any time step seems reasonable to attain a maximal precision by a given numerical effort. In particular, the boundaries between different eddy current regions should be finely resolved, since $|\nabla a|$ takes on large values there. A disadvantage of the fixed mesh for the electromagnetic fields is the necessity to consider the convective term $v \times \mathrm{curl}\, a$ explicitly in the weak form of the field equations, where v denotes the velocity field of the structure. In case of a moving mesh, this term can be implicitely considered by replacing the time derivative of a by its complete differential [29]. But this drawback is compensated by the aforementioned advantages, particularly since the corresponding Péclet-number is small such that the influence of the convective term does not affect the stability of the method.

The time integration of the electromagnetic field relations was carried out using the generalized trapezoidal rule, and that of the momentum balance using Newmark's method. Using these methods, choice of the optimal parameter values provided an accuracy of $O(\Delta t^2)$, where Δt denotes the size of the time step. At the beginning of, as well as at several instances during the numerical solution, the parameter values of the trapezoidal rule are modified in order to avoid unphysical oscillations of the time derivative of the vector potential a. In particular, such oscillations occur at the beginning of the simulation due to the switching on of the input current.

Consider next the staggered solution scheme. At the start, the magnetic field distribution is calculated with respect to the position and velocity of the structure in the nth time step. Then, the new position of the structure is determined such that a balance between inner and outer forces arises. Benchmark simulations have shown that this algorithm can be improved by adding an additional iteration loop. To ensure that the computed momentum balance of the structure in the $(n + 1)$st time step represents a balance between the Lorentz forces in the $(n + 1)$st time step and the inner forces of the structure at this instant, the following scheme is applied. Let all values having index n be variables of the nth time step. Then, the update for the $(n + 1)$st time step takes the following form:

1. A predictor value $a_1^{(n+1)}$ for the vector potential and for its time derivative in the $(n + 1)$st step is computed according to the measured amperage in the tool coil at time $t^{(n+1)}$ and the kinematic state of the work-piece that it attained when the momentum balance was reached in the nth time step. For this, the assembly routine of the magnetic mesh checks wether a certain point lies in the work-piece or not. The values for conductivity and for the velocity of the structur (for the convective term $v \times \mathrm{curl}\, a$) are chosen respectively.

2. The stiffness matrix and load vector in the work-piece mesh are assembled. For this, the nodal values for the current Lorentz force density

$$f_{\mathrm{L}1}^{(n+1)} = j_1^{(n+1)} \times b_1^{(n+1)} = \sigma_{\mathrm{EM}} \partial a_1^{(n+1)} \times \mathrm{curl}\, a_1^{(n+1)}$$

are computed.

3. The assembled equation in the work-piece mesh is solved. The computed deformations are added to the vertex positions of the work-piece mesh. It is checked whether the

residual force associated with the resulting state of deformation is zero in the scope of the desired accuracy. If the latter is false another step of the Newton-Raphson iteration has to be performed with the altered position of the work-piece. Otherwise, the vector potential $a_2^{(n+1)}$ is computed according to the new kinematic state of the structure. If it does not deviate from $a_1^{(n+1)}$ within the scope of accuracy the next time step is started. Otherwise, the equilibrium position of the structure with respect to outer forces resulting from $a_2^{(n+1)}$ and its time derivative is determined.

4. A series of vector potentials $a_k^{(n+1)}$ and corresponding equilibrium positions of the mechanical structure is computed, until $a_{k+1}^{(n+1)} = a_k^{(n+1)}$ within the scope of accuracy. Then, a new time step is started.

4 Applications

In this section, the model implementation into SOFAR as discussed in the last two sections is applied to the case of sheet metal forming. Here, the work-piece consists of the aluminum alloy AC120. For this material, the semi-empirical form

$$-\eta_P(\epsilon_P) = \sigma_{F0}\,\epsilon_P + c_1\,(\epsilon_P + c_2)^{c_3} + c_4\,\ln(1 + c_5\,\epsilon_P) \tag{13}$$

was assumed for the inelastic specific entropy $\psi_P(\epsilon_P)$ due to energy storage in the material resulting from quasi-static isotropic hardening. In particular, the room-temperature data of [7] for AC120 yielded σ_{F0} = 116.0 MPa, c_1 = −12.39 MPa, c_2 = 0.001, c_3 = 0.0697, c_4 = 80.31 MPa and c_5 = 36.59. Since experimental identification of the remaining dynamic viscoplastic parameters σ_P, γ_P and m_P represents work in progress, the values σ_{Pr} = 90 MPa, γ_{Pr} = 200000 s^{-1} and m_{Pr} = 5 have been estimated for aluminum from the literature (*e.g.*[30]) in the high strain-rate regime (*i.e.*$|D| > 10^3$ s^{-1}). As indicated by the results of the last section, generally speaking, these are all a function of temperature, accumulated inelastic strain, and strain rate. Indeed, in the conventional forming regime (*i.e.*, 10^{-1} s$^{-1} < |D| < 10^3$ s^{-1}), one may estimate σ_P = 100 MPa, γ_{Pr} = 6500 s^{-1} and m_{Pr} = 4 in a similar fashion. Remaining parameter values assumed at θ_r = 298 K include λ_r = 39404 MPa, μ_r = 26269 MPa, α_r = 2.2 × 10^{-5} K^{-1}, ϱ_r = 2700 kg m^{-3}, and c_r = 903 J kg^{-1} K^{-1}.
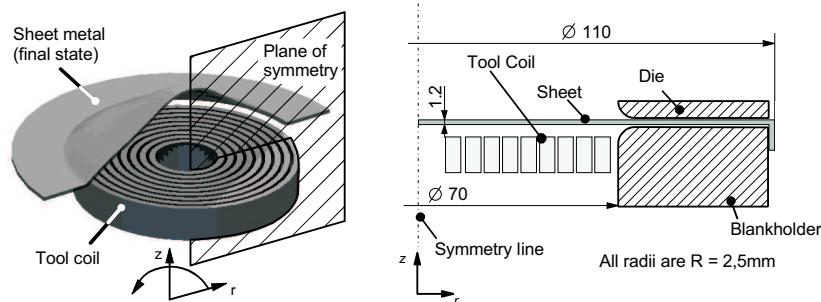

Figure 1: *Geometry of work-piece, die and tool coil for the sheet metal case.*

The simulated magnetic field development resulting in a Lorentz force in the sheet metal plate driving the forming process is shown in Figure 2. In particular, the distribution of the radial

component of the magnetic flux at 20 (above) and 80 μs (below) during forming is shown. As can be seen, after 80 μs the intensity of the magnetic flux, and so the Lorentz force has decayed significantly such that further plate deformation is driven by inertial forces alone. The forming stages corresponding to the magnetic field development in Figure 2 are displayed in Figure 3 along with the development of the accumulated inelastic deformation. At the beginning of the process, the center of the plate remains at rest. On the other hand, at r = 21 mm the plate experiences high Lorentz forces and begins to accelerate. In later stages, the center of the plate is then pulled along by the rest of the plate and accelerated via predominantly inertial forces, resulting in the cap-shaped structure at the end of the process. This is mirrored by the evolution of the accumulated inelastic strain ϵ_P which is maximal at the top of the cap.
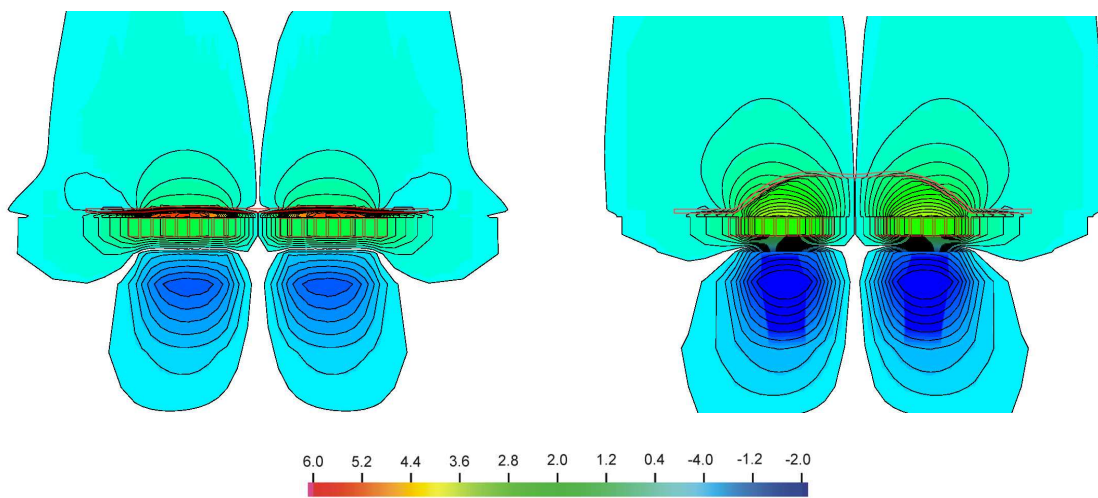

Figure 2: *Radial (i.e.horizontal) component of the magnetic flux b at 20 μs (left) and 80 μs (right). Values shown are given in Tesla. Sheet metal plate and magnetic tool coil are also shown (in red).*
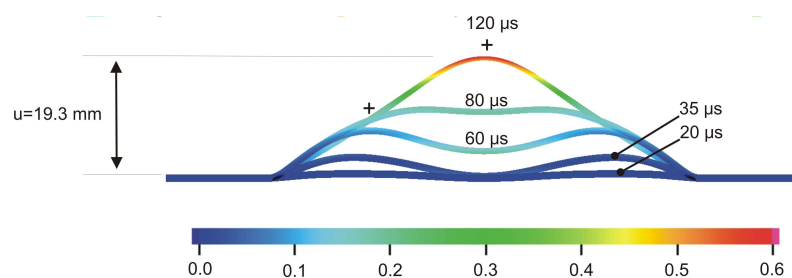

Figure 3: *Sheet metal profile and accumulated inelastic strain ϵ_P at various stages during the forming process. For comparison, corresponding experimentally-determined sheet metal heights for the final profile are shown (+).*

Comparison of the simulated and experimentally-determined sheet metal profiles in Figure 3 imply that the current simulation underestimates the amount of forming slightly. Since the corresponding elastoplastic simulation from [17] agrees exactly with the experimental heights, this discrepancy would seem to be due more to the simulation of the Lorentz force than that due to the inaccuracy of the dynamic viscoplastic parameters σ_P, γ_P and, m_P. As mentioned above, their determination represents work in progress.

5   Use of SOFAR in Computer-Aided Design Problems

A major application of the above described simulation tool is the solution of different types of optimisation problems. On one hand, the identification of material parameters requires the solution of such problems, where the objective function to be minimised measures the deviation of the simulation result to experimental data. The problem consists of finding those parameter values that minimise the objective function. On the other hand, process parameters are to be identified. Here, the objective function represents the deviation of the simulation result from a desired output of the process. Thus, the method is applied to design an optimised process. Such problems are called computer aided manufacturing problems (CAM).

For a reliable and effective performance of these optimisation problems an efficient mathematical method is necessary. An adequate choice depends on details of the regarded problem. Recently, Becker and Vexler developed a mathematical theory for the error estimation for parameter identification processes that are based on Newton's method [31].

Although the free forming of aluminum offers only limited freedom to produce a desired shape, we will regard the following *academic* problem as a test for the implemented algorithm. The forming process described in the preceding section is regarded (see Figure 1). It is parametrised by two quantities. The first of these is the radius R of the tool coil, and the second is the maximum value I of the current in the circuit of the tool coil. We assume that the shape of the current curve can be held constant by the power supply, indepent of its peak value and of the size of the tool coil (which is of course another academic assumption). Next, a finite number n of radii $0 \leq r_1 < \ldots < r_n$ is chosen and n values $y_1, \ldots, y_n$ representing the height of the deformed work-piece at these radii are prescribed. We are now interested in finding those parameter values that minimise

$$f(R, I) = \sum_{i=1}^{n} (h(r_i) - y_i)^2 \tag{14}$$

where $h(r)$ describes the height of the deformed work piece at the radius r. As optimisation algorithm the Nelder-Mead simplex search is taken [18]. It is a direct search method that does not require gradients or other derivative information. At each step of the search a new point in or near the current simplex is generated according to a simple algorithm. The function value at the new point is compared with the function's values at the vertices of the simplex and, usually, one of the vertices is replaced by the new point, giving a new simplex. If a certain point x has been maintained as simplex vertex during a specified number of steps, the simplex is shrinked by a certain scaling factor such that x remains a vertex of the smaller simplex. These steps are repeated until the diameter of the simplex is less than the specified tolerance.

6   Conclusions

A multifield model for coupled electromagnetic thermomechanical composite systems has been implemented in the object oriented finite-element software environment SOFAR. The corresponding simulation tool has been applied to the case of electromagnetic sheet metal forming and used for parameter identification as well as process optimisation. The particular algorithmic implementation utilised in SOFAR has been developed with the help of a set of benchmark

tests applied to different cases of EF. The unification of coupled multifield simulation problems such as EF in a single software environment like SOFAR makes it possible to achieve more reliable, numerically-efficient and robust simulations which take advantage of the most recent advances in element technology and numerical methods, something of crucial importance to further development and improvement of such simulations.

References

[1] *W. H. Gourdin.* Analysis and assessment of electromagnetic ring expansion as a high-strain rate test. *J. Appl. Phys.*, 65:411, 1989.

[2] *W. H. Gourdin, S. L. Weinland, and R. M. Boling.* Development of the electromagnetically-launched expanding ring as a high strain-rate test. *Rev. Sci. Instrum.*, 60:427, 1989.

[3] *N. Takata, M. Kato, K. Sato, and T. Tobe.* High-speed forming of metal sheets by electromagnetic forces. *Japan Soc. Mech. Eng. Int. J.*, 31:142, 1988.

[4] *G. Fenton and G. S. Daehn.* Modeling of electromagnetically formed sheet metal. *J. Mat. Process. Tech.*, 75:6–16, 1998.

[5] *R. Tipton.* *CALE User's Manual.* Lawrence Livermore National Laboratory, 1992.

[6] *C. Beerwald, A. Brosius, W. Homberg, M. Kleiner, and A. Wellendorf.* New aspects of electromagnetic forming. In *Proceedings of the 6th International Conference on the Technology of Plasticity*, volume III, pages 2471–2476, 1999.

[7] *C. Beerwald, A. Brosius, and M. Kleiner.* Determination of flow stress at very high strain-rates by a combination of magnetic forming and fem calculation. In *Proceedings of the International Workshop on Friction and Flow Stress in Cutting and Forming (CIRP).* ENSAM - Paris, 2000.

[8] *MSC.Software.Cooperation.* Marc, version 2001, 2001.

[9] *M. Badelt, C. Beerwald, A Brosius, and M. Kleiner.* Process analysis of electromagnetic sheet metal forming by online-measurement and finite element simulation. In *Proceedings of the 6th International ESAFORM Conference on Material Forming, 28.-30. April 2003, Italy*, pages 123–126. ESAFORM 2003, 2002.

[10] *C. Beerwald, A. Brosius, W. Homberg, M. Kleiner, M. Klocke, and S. Kulig.* Extended finite element modelling of electromagnetic forming. In *Proceedings of the 10th International Conference, 14.-16. April 2003, United Kingdom*, pages 559–566. SheetMetal 2003, 2003.

[11] *D. Meeker.* Femm, version 3.2, 2002.

[12] *Ansoft Corporation.* Emas, version 4.0, 1999.

[13] *H. Blum, H. Kleemann, A. Rademacher, T. Rauscher, A. Schroeder, and M. Stiemer.* SOFAR. www.mathematik.uni-dortmund.de/lsx/sofar, 2003.

[14] *B. Svendsen and T. Chanda.* Continuum thermodynamic modeling and simulation of electromagnetic metal forming. *Technische Mechanik*, 23:103–112, 2003.

[15] *B. Svendsen and T. Chanda.* Continuum thermodynamic formulation of models for electromagnetic thermoinelastic materials with application to electromagnetic metal forming. *Cont. Mech. Thermodyn.*, 2004. submitted.

[16] *M. Stiemer, J. Unger, H. Blum, B. Svendsen.* Algorithmic formulation and numerical implementation of coupled multifield models for electromagnetic metal forming simulations. in preparation, 2004.

[17] *M. Kleiner, A. Brosius, H. Blum, F. T. Suttmeier, M. Stiemer, B. Svendsen, J. Unger, S. Reese.* Benchmark simulation for coupled electromagnetic-mechanical metal forming processes. Annals of the German Society for Production Technology, in press, 2004.

[18] *J. A. Nelder and R. Mead.* A simplex method for function minimization. *Computer J.*, 7:308–313.

[19] *F. Moon. Magnetic interactions in solids.* Springer-Verlag, 1980.

[20] *J. D. Jackson. Classical Electrodynamics.* John Wiley and Sons, 1975.

[21] *J. Lubliner.* On the thermodynamic foundation of solid mechanics. *J. Nonlinear Mech.*, 7:237–250, 1972.

[22] *P. Rosakis, A. J. Rosakis, G. Ravichandran, and J. Hodowany.* A thermodynamic internal variable model for the partition of plastic work into heat and stored energy in metals. *J. Mech. Phys. Solids*, 48:581–607, 2000.

[23] *C. Teodosiu.* Dislocation modeling of crystalline plasticity, in *Large plastic deformation of crystalline aggregates*, C. Teodosiu, ed., CISM V. 376, pp. 21–80, Springer, 1997.

[24] *B. Svendsen.* On the modeling of anisotropic elastic and inelastic material behaviour at large deformation. *Int. J. Solids Structures*, 38:9579–9599, 2001.

[25] *S. Reese and B. Svendsen.* On the modeling of internal variables as structure tensors in anisotropic, finite-deformation inelasticity. *J. de Physique IV*, 14, 2003.

[26] *B. Svendsen and S. Reese.* On the modeling of internal variables as structure tensors in anisotropic, finite-deformation inelasticity. *Int. J. Plasticity*, 2004. accepted.

[27] *J. C. Nédélec.* Mixed finite elements in $\mathbb{R}^3$. *Numerische Mathematik*, 35:315–341, 1980.

[28] *J. C. Nédélec.* A new family of mixed finite elements in $\mathbb{R}^3$. *Numerische Mathematik*, 50:57–81, 1986.

[29] *M. Schinnerl, J. Schöberl, M. Kaltenbacher, and R. Lerch.* Multigrid methods for the 3d simulation of nonlinear magneto-mechanical systems. *IEEE transactions magnetics*, 38:1497–1511, 2002.

[30] *N. Jones. Structural Impact.* Cambridge University Press, 1989.

[31] *R. Becker and B. Vexler.* Adaptive finite element methods for parameter identification problems. Preprint, University of Heidelberg.